Edinburgh Research Explorer

pH and redox dual responsive carrier-free anticancer drug nanoparticles for targeted delivery and synergistic therapy

Accepted Manuscript

pH and redox dual responsive carrier-free anticancer drug nanoparticles for targeted delivery and synergistic therapy

Mengjiao Zhou, Weijia Wei, Xianfeng Chen, Xiuzhen Xu, Xiaohong Zhang, Xiujuan Zhang
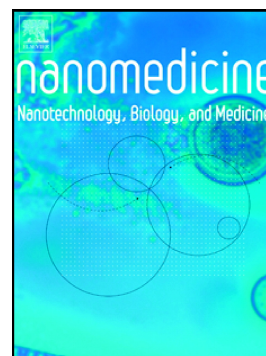
Please cite this article as: M. Zhou, W. Wei, X. Chen, et al., pH and redox dual responsive carrier-free anticancer drug nanoparticles for targeted delivery and synergistic therapy, Nanomedicine: Nanotechnology, Biology, and Medicine, https://doi.org/10.1016/j.nano.2019.04.011

pH and redox dual responsive carrier-free anticancer drug nanoparticles for targeted delivery and synergistic therapy

Mengjiao Zhou PhD[a,b], Weijia Wei MS[a], Xianfeng Chen PhD[c], Xiuzhen Xu PhD[a], Xiaohong Zhang PhD[a], Xiujuan Zhang PhD[a,*]

[a]Institute of Functional Nano & Soft Materials (FUNSOM), Jiangsu Key Laboratory for Carbon-Based Functional Materials & Devices, Soochow University, 199 Ren'ai Road, Suzhou, 215123, Jiangsu, PR China

[b]School of Pharmacy, Nantong University, 19 Qixiu Road, Nantong, 226001, Jiangsu, PR China

[c]School of Engineering, Institute for Bioengineering, The University of Edinburgh, King's Buildings, Mayfield Road, Edinburgh EH9 3JL, United Kingdom

[*]Corresponding author: (X. J. Z.) Tel: +86-512-65880955 Email: xjzhang@suda.edu.cn.

word count for the abstract: 149

complete manuscript word count: 4997

number of references: 41

number of figures/tables: 7

Abstract

Advanced drug delivery systems often employ nanomaterials as carriers to deliver drugs to desirable disease sites for enhanced efficacy. However, most systems have low drug loading capacity and cause safety concerns. Therefore, many anticancer therapeutics have recently been assembled to NPs form without using any additional nanocarrier to achieve high drug loading. However, carrier-free nanomedicines are often constrained by limitations such as inadequate stability and lack of control in drug release. Therefore, we synthesize carrier-free drug NPs containing cis-aconitic anhydride-modified doxorubicin and paclitaxel (CAD-PTX) and coating with crosslinked (CL) surfactant based on hyaluronic acid (HA) segment. With this design, the pure drug NPs possess pH and redox dual responsive release characteristic and could target CD44 overexpressed cancer cells. Our studies demonstrate that these CAD-PTX-CLHA NPs display high stability, excellent active targeting effect and controllable intracellular drug release, and ultimately achieve significantly better anti-cancer efficiency than individual doxorubicin and paclitaxel.

Keywords: Nanomedicine, pH-responsive, GSH-responsive, targeted delivery, synergistic therapy

Background

In the past a few decades, the development of nanotechnology has offered abundant opportunities for cancer therapy.[1-5] Nano-drug delivery systems have shown many superiorities compared to traditional anticancer drugs, such as controlled delivery and release, improved water-solubility, bioavailability, stability, and tumor selectivity, as well as reduced

2

side effects.[6-12] Recently, pure anticancer drug nanoparticles (NPs) have been synthesized as a new pattern of nanomedicine, which first involves assembling pure hydrophobic drugs into NPs, followed by stabilizing with surfactants for good water dispersity and high biostability.[13] These pure therapeutic NPs have high drug loading capacity and alleviate the potential systemic toxicity caused by accumulation of excipient nanocarriers such as gold and silica NPs for drug delivery.[14] However, at the current stage, the reported pure drug NPs often possess inadequate *in vivo* stability and less control of drug release depending on environment.[15] Therefore, we aim to develop environmentally responsive pure drug nanomedicine with high stability for enhanced anticancer therapy. Because of the unique pH and redox environment of tumor tissues and intracellular compartments, we decide to adopt pH and redox as the stimuli. In detail, the pH value of normal physiological condition is ~7.4, which is higher than that of tumor tissues (~6.8); the pH values of intracellular endosome and lysosome (pH 5.0-6.5) are significantly lower than those of extracellular microenvironment.[16-18] Meanwhile, glutathione (GSH) is a thiol containing tripeptide and has high concentration in cells (~ 10 mM), much higher than that of the extracellular environment (~2 μM).[19] GSH can exist in reduced state and oxidized state and therefore provides a redox environment. Therefore, joint pH and redox responsive drug delivery systems have been widely developed for controllable anticancer therapy.

With this idea, we design to synthesize pH-responsive cis-aconitic anhydride (CA)-modified doxorubicin (DOX) (CAD) and paclitaxel (PTX) NPs, followed by coating with a layer of GSH-responsive crosslinked surfactant based on sodium hyaluronic acid (HA). In the design, DOX and PTX molecules are conjugated via a pH-responsive linker CA.

3

Since DOX and PTX have different inhibition mechanisms and antitumor targets, the combination will greatly enhance therapeutic efficacy and better overcome multidrug resistance (MDR).[20-26] HA is able to target cancer cells with overexpression of CD44 receptor such as human breast adenocarcinoma cells and human lung cancer cells.[27-30] Moreover, redox induced fragmentation of disulfide bonds in HA crosslinking would consume intracellular GSH, generate cellular reactive oxygen species (ROS), and finally induce MCF-7/ADR cell apoptosis.[31-34] To confirm these NPs' pH- and redox-responsive characteristics and their efficiency in anticancer therapy, we systematically investigate their physical and chemical properties, and study the *in vitro* and *in vivo* applications.

Methods

Materials, characterization, synthesis of CAD and SAD, synthesis of CAD-PTX and SAD-PTX, synthesis of Cys_m-HA-$C18_n$ are described in Supplementary Material.

Preparation and modification of CAD-PTX NPs and SAD-PTX NPs

CAD-PTX NPs were prepared by a solvent exchange method. CAD-PTX was dissolved in DMF and then the solution was dropwisely added into water under vigorous stirring, followed by dialysis against deionized water to obtain CAD-PTX NPs. Then 200 μL of 1.0 mg mL^{-1} Cys_m-HA-$C18_n$ aqueous solution were added to the solution of CAD-PTX NPs. The mixture was then ultrasonicated for 5 min followed by 1 h incubation at room temperature to obtain CAD-PTX NCLHA NPs. To obtain NPs with crosslinked surfactants on the surface, the pH of CAD-PTX NCLHA NPs solution was adjusted to be 8.5 followed by 12 h incubation. SAD-PTX NCLHA NPs and SAD-PTX CLHA NPs were prepared with the same

method.

Stability

The stability of CAD-PTX NCLHA NPs, CAD-PTX CLHA NPs, SAD-PTX NCLHA NPs and SAD-PTX CLHA NPs was studied by using DLS to measure their size evolution in phosphate buffered solution (PBS) and fetal bovine serum (FBS) at different periods of storage. Three samples were measured in each group, and the measurements were performed in triplicate and the average was used in analysis.

In vitro release of DOX from NPs

The release of DOX from CAD-PTX-CLHA NPs were studied by placing 4 samples in separate dialysis cartridges with a 14 kDa MWCO, followed by dialysis against 100 mL of PBS/FBS (10 mM, pH 7.4), 100 mL PBS/FBS (10 mM, pH 7.4) with 10 mM DTT, 100 mL PBS/FBS (10 mM, pH 5.0), and 100 mL PBS/FBS (10 mM, pH 5.0) with 10 mM DTT at 37 °C. To determine the release, 1 mL of PBS/FBS solution was collected to measure the fluorescence of DOX. Each time after sample collection, 1 mL of fresh dialysis medium was added to each group to keep the total volume constant. Three samples were measured in each group, and the measurements were performed in triplicate and the average was used in analysis.

Cell culture

Human cervical (HeLa) cells, human embryonic kidney (HEK-293T) cells and human lung carcinoma (A549) cells were cultured in Dulbecco's Modified Eagle's medium

(DMEM), while murine 4T1 breast cancer (4T1) cells, human mammary carcinoma (MCF-7) cells and DOX resistant human mammary carcinoma (MCF-7/ADR) cells were cultured in Roswell Park Memorial Institute (RPMI) 1640 medium containing 10% of fetal bovine serum (FBS) and antibiotics in a humidified atmosphere containing 5% CO_2 at 37 °C.

In vitro cytotoxicity of NPs

The cytotoxicities of CAD-PTX-CLHA NPs and SAD-PTX-CLHA NPs were examined with a MTT assay towards HEK-293T and A549 cells. The cells pre-treated with HA polymer (5 mg/mL) for 4 h were set as control. The cells were seeded in 96-well plates at 6.0 $\times 10^4$ cells per well in 80.0 μL of complete media, and then incubated at 37 °C in 5% (v/v) CO_2 for 24 h. The drug concentrations of CAD-PTX-CLHA NPs were ranged from 2.5 to 40 μM (2.5, 5, 10, 20 and 40 μM). The drug concentration (DC) was defined as the sum concentration of DOX and PTX in each well. After incubation for another 24 h and 48 h, the standard MTT assay was performed to determine the viability of cells. Six cell samples were measured in each group for averaged calculation.

Subsequently, the cytotoxicities of DOX·HCl, PTX, DOX+PTX mixture, CAD-PTX-NCLHA NPs, CAD-PTX-CLHA NPs, SAD-PTX-NCLHA NPs and SAD-PTX-CLHA NPs towards HeLa and 4T1 cells were measured. Samples were added to each well with a drug concentration from 2.5 to 40 μM (2.5, 5, 10, 20 and 40 μM). In a separate experiment, the inhibition effect of multidrug resistance was examined with a MTT assay towards MCF-7/ADR cells expressing a high level of CD44 receptors. DOX·HCl, DOX+PTX mixture and CAD-PTX-CLHA NPs were added to each well. The DC was 2.5, 5,

6

10, 20 and 40 μM in different groups. In another experiment, the cells were pre-treated with HA polymer (5 mg/mL) for 4 h, then CAD-PTX-CLHA NPs of different concentrations were added to each well. Six cell samples were measured in each group for averaged calculation.

In vitro cellular uptake

The intracellular distribution of CAD-PTX-CLHA NPs in HeLa cells was observed using confocal laser scanning microscopy (CLSM). HeLa cells were seeded in a 24-well plate at a density of 1.0×10^5 cells per well in 0.8 mL of complete media and incubated for 12 h. Next, 200 μL of CAD-PTX-CLHA NPs were added to each well (5.0 μM of DOX). After cells were incubated with CAD-PTX-CLHA NPs for different times (4, 6, 12 and 24 h). Hoechst 33258 and Lyso-Tracker Green (Beyotime, Shanghai agent, China) were used to stain the nuclei and lysosome of cells for 30 min under 5% CO_2, respectively. Finally, the cells were washed with PBS for three times and studied using a Leica laser scanning confocal microscope.

The cellular uptake of CAD-PTX-CLHA NPs were studied in MCF-7/ADR cells using both CLSM and flow cytometry. In the experiment, 200 μL of DOX·HCl or CAD-PTX-CLHA NPs were added to each well (5.0 μM of DOX), followed by incubation at 37 °C for 6 and 12 h. Then the cells were washed with PBS for three times and stained with Lyso-Tracker Green for 30 min under 5% CO_2 at 37 °C. Finally, the cells were again washed with PBS for three times for confocal fluorescence microscopy imaging. Additionally, extra groups of cells treated with the same way as above were trypsinized for flow cytometry analysis. For both CLSM and flow cytometry analysis, the inhibition experiments were also

7

performed by pre-treating MCF-7/ADR cells with free HA (5 mg/mL) for 4 h prior to incubating with CAD-PTX-CLHA NPs.

Detection of ROS

MCF-7/ADR cells were treated with blank cell culture medium and medium containing DOX·HCl, PTX, DOX+PTX mixture, and CAD-PTX-CLHA NPs under 5% CO_2 at 37 °C. After 12 and 24 h incubation, the culture medium was removed and the cells were washed with PBS for two times, followed by staining with DCFH-DA (Beyotime, Shanghai agent, China) for 20 min under 5% CO_2 at 37 °C for confocal fluorescence microscopy. The total concentrations of DOX and PTX in all groups were 10 μM.

In vivo blood circulation of CAD-PTX-CLHA NPs

To know the blood circulation of CAD-PTX-CLHA NPs, samples were injected into BALB/c mice via intravenous tail vein injection (200 μL, 1 mg/mL). At each desirable time point after injection, ~10 μL of blood was collected, followed by dissolving in 1 mL of lysis buffer (1% SDS, 1% Triton X-100, 40 mM Tris acetate) to measure the fluorescence intensity of DOX. Five mice were measured in each group for averaged calculation.

Biodistribution of CAD-PTX-CLHA NPs

The biodistribution of CAD-PTX-CLHA NPs after intravenous injections were qualitatively or semiquantitatively assessed by *ex vivo* CAD-PTX fluorescence imaging of major internal organs. In detail, tumor bearing mice were prepared by inoculating MCF-7/ADR cells into BALB/c mice. When the tumor volume increased to about 50 mm³,

8

200 µL of CAD-PTX-CLHA NPs (1 mg/mL) were intravenously injected to mice though tail vain. The mice were sacrificed at different time intervals (2, 6, 12 and 24 h), and the major organs including heart, liver, spleen, lung, kidney, stomach, intestine and tumor were excised for fluorescence imaging. The background signal and autofluorescence of individual tissues and organs of untreated mice were used as a reference. Three mice were measured in each group for averaged calculation.

In vivo imaging

The hair of MCF-7/ADR tumor-bearing mice was removed from neck to foot, followed by intravenous injection of 200 µL of 1 mg/mL CAD-PTX-CLHA NPs. After 24 h, the mice were imaged using a Maestro *in vivo* fluorescence imaging system (CRi Inc.), using a 488 nm laser as the excitation source. *In vivo* spectral imaging (10 nm step) was carried out from 520 to 650 nm for the mice.

In vivo antitumor activity

Individual groups of MCF-7/ADR tumor-bearing mice were separately treated with 200 µL of PBS, and 1 mg/ml of DOX·HCl, PTX, DOX+PTX mixture and CAD-PTX-CLHA NPs. A boost injection was given at 7 days after the primary injection. The tumor size and weight of each mouse were measured daily for 2 weeks. Relative tumor size and weight were calculated to be the ratio of tumor volume and weight over the initial values, respectively, immediately before the primary treatment. All animal experiments were performed with the approval of Soochow University Laboratory Animal Center and the Animal Care and Use Committee of Soochow University. Six mice were measured in each group for averaged

9

calculation.

Results

Synthesis and characterization of CAD-PTX, SAD-PTX and Cys_7-HA-$C18_4$

To develop pH-responsive dimeric drug molecules, DOX and PTX were conjugated *via* CA as the bridge to produce CAD-PTX. The synthetic route is depicted in Figure 1, *A*. Due to the influence of the α-ethylenic bond, the amide bond between DOX and CA is pH-responsive. For comparison, SAD-PTX molecules conjugated by SA were also developed (Figure S1) to be responsive to pH values. The ^{1}H NMR spectrum of CAD (Figure S2, *A*) displays signals at 6.28 ppm attributed to the hydrogen proton in CA, while the signals at 2.31-2.37 ppm in the ^{1}H NMR spectrum of SAD (Figure S2, *B*) can be attributed to the hydrogen proton in SA. Moreover, the signals of the hydrogen protons in DOX and PTX are shown in the ^{1}H NMR spectra of CAD-PTX and SAD-PTX, respectively.

To allow drug NPs to be responsive to redox environment, a surfactant was synthesized containing hydrophobic segments (C18), crosslinkable cysteine (Cys) and hydrophilic HA, termed Cys_m-HA-$C18_n$. HA is redox responsive and can effectively target the CD44 receptor overexpressing on cancer cells. The synthetic route of Cys_m-HA-$C18_n$ is illustrated in Figure 1, *B*. The ^{1}H NMR spectrum of Cys_m-HA-$C18_n$ is shown in Figure S3. The ^{1}H NMR spectrum exhibits clear signals attributable to Cys moieties (δ 2.56, 3.12-3.18), C18 segments (1.22) and HA backbone (δ 1.93, 3.25-3.95, 4.50). The degree of substitution (DS) is defined as the number of C18 or Cys units per

10

100 sugar residues of HA polymer. The DS of C18 could be determined by calculating the integrals of signals at δ 1.22 (methylene protons of Lys) and δ 4.50 (anomeric proton in HA). Herein, the DS of C18 is 4, and the DS of Cys determined by Ellman's test is 7. Thus, the molecular formula of our synthesized surfactant is Cys_7-HA-$C18_4$.

To enable Cys_7-HA-$C18_4$ molecules to crosslink, the pH value of the solution was adjusted to be 8.5. The free thiol groups in the solution were determined by Ellman's test. As shown in Figure 3, *D*, the absorbance of the free thiol groups in the solution (pH 8.5) disappears after 12 h reaction.

Preparation and characterization of NPs

CAD-PTX NPs were synthesized via a solvent exchange method (Figure 2). Subsequently, Cys_7-HA-$C18_4$ aqueous solution was added to CAD-PTX NPs suspension for surface coating. On these NPs, the surfactant molecules are not cross-linked (NCL), termed as CAD-PTX-NCLHA NPs. Our previous work has shown that NPs stability can be substantially enhanced when surfactant molecules are crosslinked, which will prevent premature release of drugs during blood circulation.[35] Therefore, to improve the stability of CAD-PTX-NCLHA NPs, Cys_7-HA-$C18_4$ molecules were cross-linked by adjusting the solution pH to be 8.5 followed by 12 h incubation. These NPs with crosslinked surfactant molecules are defined as CAD-PTX-CLHA NPs. As control groups, SAD-PTX NCLHA NPs and SAD-PTX CLHA NPs were also prepared with similar procedures.

The as-prepared NPs were observed with scanning electron microscopy (SEM) and transmission electron microscopy (TEM). The results indicate that CAD-PTX (Figure 3, *A*) and SAD-PTX (Figure S4, *A*) NPs are spherical and have relatively uniform size. The hydrodynamic sizes of the NPs were measured by DLS analysis and the results are shown in Figure 3, *B* and Figure S4. The average sizes of CAD-PTX and SAD-PTX NPs are approximately 90 nm. After surface modification with Cys_7-HA-$C18_4$, the size of the NPs does not change much regardless of whether the surfactant molecules are crosslinked or not. The stability of these NPs in PBS and FBS is also studied (Figure 3, *C*, Figure S5 and Figure S6). Apparently, with Cys_7-HA-$C18_4$ molecules coated on the surface of NPs, whether they are cross-linked or not, the surface-functionalized NPs both display good stability. We further measured the release rate of free DOX and CAD-PTX-CLHA NPs. As Figure S7 shown, DOX was rapidly released from free DOX, however, the drug release rate of CAD-PTX-CLHA NPs was significantly slower at neutral pH, confirming NPs' stability in physiological environment.

After synthesizing CAD-PTX-CLHA NPs, it is important to know their drug release profiles. As shown in Figure 3, *E* and *F*, within the first 10 h, no burst release is observed from both CAD-PTX-CLHA NPs and SAD-PTX-CLHA NPs, with only approximately 13% and 12% of DOX is released in PBS at pH 7.4, respectively. With decrease of pH values from 7.4 to 5.0, the cumulative DOX release amount of CAD-PTX-CLHA NPs is significantly accelerated to 34% within the same period, while that of SAD-PTX-CLHA NPs is only 15%. The burst release of DOX from

12

CAD-PTX-CLHA NPs at pH 5.0 may be due to the breakage of pH-sensitive linkage under acidic environment.

Attractively, the release of DOX from CAD-PTX-CLHA and SAD-PTX-CLHA NPs can be boosted under a redox environment containing 10 mM DTT. Within the first 10 h, at pH 7.4, 30% and 28% of DOX is released from CAD-PTX-CLHA and SAD-PTX-CLHA NPs, respectively. Compared with the case without DTT, the DOX release from both types of NPs has been more than doubled. At pH 5.0 and 10 mM DTT, the release of DOX from CAD-PTX-CLHA NPs dramatically increases to 68% within the same period of time. In great contrast, under the same condition of pH and redox environment, only 30% of DOX is released from SAD-PTX-CLHA NPs. Furthermore, the drug release profiles of NPs in FBS solution are also investigated (Figure S8). Compared with FBS at pH 7.4, the release of DOX from CAD-PTX-CLHA NPs increases apparently at pH 5.0 and 10 mM DTT, which is consistent with that in PBS solutions.

Cellular uptake and intracellular distribution of NPs

After knowing the release profile of CAD-PTX-CLHA NPs, we further studied their intracellular release kinetics. As shown in Figure 4, at 4 h after HeLa cells being incubated with CAD-PTX-CLHA NPs, very weak red fluorescence of DOX can be observed in the cytoplasm. As time increases, by the 12 h time point, the fluorescence signal becomes stronger and gradually migrates to the nuclei region. After 24 h incubation, intense DOX fluorescence overlaps with the nuclei staining. These results

are possibly due to the behaviour that CAD-PTX-CLHA NPs release DOX in the acidic intracellular pathway compartments, and subsequently diffuse to the nuclei region.

In vitro cytotoxicity of NPs

To verify the targeting ability of CAD-PTX-CLHA NPs, HEK-293T normal cells expressing a low level of CD44 receptors, and A549 cancer cells overexpressing with CD44 receptors were chosen as model cells.[36] Additionally, another group of A549 cancer cells was pre-treated with HA for 4 hours and used as control group. As presented in Figure 5, *A* and *B*, CAD-PTX-CLHA NPs show time and dose dependent cytotoxicity to the tested three cell lines. At the highest concentration of 40 µM, CAD-PTX-CLHA NPs still exhibit low cytotoxicity (viability of 72%) against HEK-293T normal cells, but the cytotoxicity to A549 cancer cells is much higher, with a viability of 23%. Attractively, when A549 cancer cells was pre-treated with HA for 4 hours, CAD-PTX-CLHA NPs with the same concentration exhibit a much lower cytotoxicity (viability of 67%). The reason is that the surface CD44 receptors have been conjugated with HA in the pre-treatment. Therefore, the CAD-PTX-CLHA NPs were not able to effectively target these cells any more. Besides, the *in vitro* cytotoxicity of SAD-PTX-CLHA NPs are also measured. As shown in Figure S9, HA pre-treated A549 cancer cells prevents their internalization of SAD-PTX-CLHA NPs, further demonstrating that CAD-PTX-CLHA NPs targeting A549 cancer cells mainly through CD44.

To further explore the cancer cell killing effect, CAD-PTX-CLHA NPs of different drug concentrations ranging from 2.5 to 40 μM were incubated with HeLa and 4T1 cells for 48 hours, followed by viability measurement (Figure 5, *C* and *D*, and Figure S10). DOX·HCl, PTX, DOX+PTX mixture, and CAD-PTX-NCLHA NPs were also tested under the same conditions for comparison. The concentrations were defined as the sum concentration of DOX and PTX in each sample. As shown in Figure 5, *C*, at the highest concentration of 40 μM, CAD-PTX-CLHA NPs have higher cytotoxicity (viability of only 10%) than all other reagents: the viabilities of DOX, PTX, and DOX-PTX, and CAD-PTX-NCLHA NPs treated cells are 21%, 26%, 23%, and 9%, respectively.

Besides, at all concentrations, CAD-PTX NPs possess higher toxicity than SAD-PTX NPs, which may be resulted from the quick release of DOX from CAD-PTX NPs at acidic intracellular microenvironment (Figure 5, *C* and *D*, Figure S11 and S12). For example, at the highest drug concentration of 40 μM, CAD-PTX-CLHA NPs exhibit substantially higher cytotoxicity (viability of 10%) than SAD-PTX-CLHA NPs (viability of about 50-60%).

To study the inhibition effect towards multidrug resistant cells, CAD-PTX-CLHA NPs were incubated with MCF-7/ADR cells, followed by viability examination. MCF-7 cells were also used in another group as control (Figure 5, *E* and *F*, Figure S13). At the highest drug concentration of 40 μM, CAD-PTX-CLHA NPs possess similar toxicity against MCF-7 cells with DOX and DOX+PTX mixture. However, when incubated with MCF-7/ADR cells, CAD-PTX-CLHA NPs exhibit apparently higher

15

toxicity than free drug groups, indicating their effective efficacy in killing multidrug resistant cells. The targeting performance of CAD-PTX-CLHA NPs towards MCF-7/ADR cells which express a high level of CD44 receptors was also investigated. After being pre-treated with HA polymer (5 mg/mL) for 4 h, MCF-7/ADR cells were incubated with different concentrations of CAD-PTX-CLHA NPs. As displayed in Figure S14, the cytotoxicity of CAD-PTX-CLHA NPs is significantly reduced, revealing that Cys_7-HA-$C18_4$ molecules possess apparent targeting ability to CD44-positive cells.

Alleviating multidrug resistance with CAD-PTX-CLHA NPs

To study the possible reasons why CAD-PTX-CLHA NPs are able to alleviate drug resistance, the cellular uptake of CAD-PTX-CLHA NPs by MCF-7/ADR cells was studied by confocal fluorescence microscopy and flow cytometry. DOX·HCl was used as a control group. As shown in Figure 6, *A* and *B*, DOX·HCl treated MCF-7/ADR cells exhibit red fluorescence signal after 6 h incubation, but the fluorescence disappears after 12 h incubation, which is likely due to drug efflux or activation of coordinately regulated detoxifying systems in the cells.[37] In comparison, CAD-PTX-CLHA NPs treated MCF-7/ADR cells still display strong fluorescence after 12 h incubation. When MCF-7/ADR cells were pre-treated with HA before incubation with CAD-PTX-CLHA NPs, the fluorescence intensity in the cells becomes very low. These data confirm that CAD-PTX-CLHA NPs are uptaken by MCF-7/ADR cells *via* a receptor-mediated mechanism. The quantitative results in Figure 6, *C* and *D* showed

that the cellular uptake of CAD-PTX-CLHA NPs became stronger over time in MCF-7/ADR cells, while poor uptaken was found when MCF-7/ADR cells were pre-treated with HA, further back up the above findings.

In addition, reactive oxygen species (ROS) generation in MCF-7/ADR cells treated with different drugs were also examined. PTX can interfere with cell microtubules to block the cell reduction pathway, resulting in NADPH oxidation and increased intracellular ROS.[38] The decrosslinking of disulfide bonds on the surface of CAD-PTX-CLHA NPs would consume intracellular GSH and then improve the level of cellular ROS.[39] Ultimately, the increased intracellular ROS levels will induce cell apoptosis.[40] Due to its importance, the intracellular ROS generation was measured. As shown in Figure 6, *E*, CAD-PTX-CLHA NPs produce a large amount of ROS in MCF-7/ADR cells indicated by the strong fluorescence intensity, which is substantially higher than that generated in the cells treated with DOX·HCl, PTX and DOX+PTX mixture.

In vivo performance of CAD-PTX-CLHA NPs

Once we successfully demonstrate the advantages of pH- and redox- dual responsive CAD-PTX-CLHA NPs and their high efficacy in inhibiting cancer cells including multidrug resistant cells, the next key question is to study whether the NPs can effectively work in *in vivo* animal model. For this purpose, we investigated the blood circulation and biodistribution of these NPs and their tumor inhibition capacity in mice. The plasma levels of CAD-PTX-CLHA NPs were determined by measuring the

17

DOX amount of blood samples at different time intervals following a single injection of CAD-PTX-CLHA NPs in mice. Notably, CAD-PTX-CLHA NPs reveal a significantly long blood circulation time with a half-life of approximately 4 h (Figure S15).

To investigate whether CAD-PTX-CLHA NPs preferentially accumulate in tumor region or not, CAD-PTX-CLHA NPs were intravenously injected into MCF-7/ADR tumor-bearing BALB/C mice for *in vivo* imaging. A laser at 488 nm was used as an excitation light for DOX. As shown in Figure 7, *A*, the CAD-PTX-CLHA NPs treated mouse displays intense red fluorescence at the tumor site at 24 h after injection. This indicates that CAD-PTX-CLHA NPs possess excellent performance in tumor targeting, which can also be used for tumor diagnosis. Subsequently, to know the detailed biodistribution of these NPs, the fluorescence intensities of various organs were monitored at different time intervals after NP injection. As presented in Figure 7, *B* and Figure S16, the mice treated with CAD-PTX-CLHA NPs possess higher levels of fluorescence signals in the tumor tissue than other major organs including heart, liver, spleen, lung, kidney, stomach and intestine. Collectively, all of these outcomes exhibit that CAD-PTX-CLHA NPs have excellent tumor targeting ability, resulting high drug accumulation in tumors and potent ability in tumor growth inhibition.

To investigate the therapeutic performance of CAD-PTX-CLHA NPs, MCF-7/ADR tumor bearing nude mice were employed as model animals. The results show that the growth of tumor is effectively inhibited by CAD-PTX-CLHA NPs, with a tumor volume of 2.06 ± 0.46 fold of the starting value. In contrast, continuous tumor

growth has been observed in the mice treated with DOX·HCl (5.42 ± 0.49 fold), PTX (5.60 ± 0.50 fold), DOX+PTX mixture (4.76 ± 0.61 fold) and PBS (7.64 ± 0.66 fold) (Figure 7, *C*).

Importantly, the mice treated with CAD-PTX-CLHA NPs have little change of body weight, which is in a sharp contrast to the significant body weight loss for mice treated with DOX·HCl, PTX and DOX+PTX mixture (Figure 7, *D*).

We further investigated hematoxylin-eosin (H&E) staining of the major organs sections (heart, liver, spleen, lung, and kidney) of saline and CAD-PTX-CLHA NPs treated mice at 14 days after initial treatment (Figure S17). Compared to saline-treated control group, organs sections of CAD-PTX-CLHA NPs treated mice displayed no obvious damages or inflammatory lesion.

Discussion

With the aim to design pure anticancer NPs with controlled and environmentally responsive release for tumor targeted therapy, we prepared a pH-and redox- dual responsive DOX and PTX drug NPs. These NPs are relatively stable in neutral pH such as blood stream with very low release of drugs. In comparison, at acidic pH and redox environment, drug release is significantly increased. These results clearly indicate that CAD-PTX-CLHA NPs present a pH and redox responsive drug release characteristic (Figure 3, *E* and *F*). Intracellular distribution images indicate that the NPs can also be fluorescently monitored and used for diagnosis (Figure 4).

Moreover, CAD-PTX-CLHA NPs exhibit high cytotoxicity to A549 cancer cells

(viability of 23%) but low cytotoxicity (viability of 72%) against HEK-293T normal cells and A549 cancer cells pre-treated with HA (viability of 67%) (Figure 5, *A* and *B*), indicating that these NPs are able to target cancer cells with overexpression of CD44 receptor. Meanwhile, CAD-PTX-CLHA NPs have higher cytotoxicity (viability of only 10%) than DOX (viability of 21%) and PTX (viability of 26%) to HeLa cells at the same drug concentrations, revealing it possesses synergistic anticancer efficacy (Figure 5, *C*). However, CAD-PTX-CLHA NPs display less effectiveness than free DOX when against 4T1 cells (Figure 5, D), as peri-cellular HA matrix can prevent NPs' uptake by 4T1 cells.[41] Furthermore, intracellular distribution images show that CAD-PTX-CLHA NPs can effectively enter MCF-7/ADR cells and maintain with the cells for a long period of time, which may be accounted to the ability of alleviating multidrug resistance (Figure 6).

When tested in mice, these NPs have a long blood circulation half-life, high accumulation in tumors, and ultimately excellent inhibition of multidrug resistant tumor growth (Figure 7). Furthermore, H&E staining of the major organs demonstrate that CAD-PTX-CLHA NPs process low systemic toxicity, which is good for *in vivo* antitumor applications.

The excellent tumor inhibition of CAD-PTX-CLHA NPs should be ascribe to their collective advantages and characteristics including cancer cell targeting, synergistic therapy of DOX and PTX, pH- and redox- dual responsive release, and effective uptake and retention in multidrug resistance cells. All results suggest that our CAD-PTX-CLHA NPs process great potential for clinical cancer chemotherapy.

Supplementary data

Additional data related to this manuscript are provided in the Supplementary material.

Acknowledgements

Conflict of interest

The authors have declared that no conflict of interest exists.

References

1. Zhang Y, Cui ZF, Kong HT, Xia K, Pan L, Li J, et al. One-shot immunomodulatory nanodiamond agents for cancer immunotherapy. *Adv Mater* 2016;**28**:2699-708.

2. Chen YJ, Wu YK, Sun BB, Liu SJ, Liu HY. Two-dimensional nanomaterials for cancer nanotheranostics. *Small* 2017;**13**:1603446.

3. Banzhaf CA, Thaysen-Petersen D, Bay C, Philipsen PA, Mogensen M, Prow T, et al. Fractional laser-assisted drug uptake: impact of time-related topical application to achieve enhanced delivery. *Laser Surg Med* 2017;**49**:348-54.

4. Li L, Huh KM, Lee YK, Kim SY. Design of a multifunctional heparin-based nanoparticle system for anticancer drug delivery. *Macromol Res* 2010;**18**:153-61.

5. Torchilin V. Tumor delivery of macromolecular drugs based on the EPR effect. *Adv Drug Deliver Rev* 2011;**63**:131-5.

6. Chou HS, Hsiao MH, Hung WY, Yen TY, Lin HY, Liu DM. A pH-responsive amphiphilic chitosan-pyranine core-shell nanoparticle for controlled drug delivery, imaging and intracellular pH measurement. *J Mater Chem B* 2014;**2**:6580-9.

7. Sinha A, Chakraborty A, Jana NR. Dextran-gated, multifunctional mesoporous nanoparticle for glucose-responsive and targeted drug delivery. *ACS Appl Mater Inter* 2014;**6**:22183-91.

8. Xiao D, Jia HZ, Zhang J, Liu CW, Zhuo RX, Zhang XZ. A dual-responsive mesoporous silica nanoparticle for tumor-triggered targeting drug delivery. *Small* 2014;**10**:591-8.

9. Lee JY, Carugo D, Crake C, Owen J, de St Victor M, Seth A, et al. Nanoparticle-loaded protein-polymer nanodroplets for improved stability and conversion efficiency in ultrasound

imaging and drug delivery. *Adv Mater* 2015;**27**:5484-92.

10. Xu X, Lu S, Gao C, Wang X, Bai X, Duan H, et al. Polymeric micelle-coated mesoporous silica nanoparticle for enhanced fluorescent imaging and pH-responsive drug delivery. *Chem Eng J* 2015;**279**:851-60.

11. Mitter N, Worrall EA, Robinson KE, Li P, Jain RG, Taochy C, et al. Clay nanosheets for topical delivery of RNAi for sustained protection against plant viruses. *Nat Plants* 2017;**3**:1-11.

12. Xu LF, Wang G, Shen JL, Geng HP, Li WQ, Wu LL, et al. Structural and optical control of DNA-mediated Janus plasmonic nanostructures. *Nanoscale* 2016;**8**:9337-42

13. Li W, Yang YL, Wang C, Liu Z, Zhang XJ, An FF, et al. Carrier-free, functionalized drug nanoparticles for targeted drug delivery. *Chem Commun* 2012;**48**:8120-2.

14. Zhang J, Li Y, An FF, Zhang X, Chen X, Lee CS. Preparation and size control of sub-100 nm pure nanodrugs. *Nano Lett* 2015;**15**:313-8.

15. Ge Z, Liu S. Functional block copolymer assemblies responsive to tumor and intracellular microenvironments for site-specific drug delivery and enhanced imaging performance. *Chem Soc Rev* 2013;**42**:7289-325.

16. Ding J, Shi F, Li D, Chen L, Zhuang X, Chen X. Enhanced endocytosis of acid-sensitive doxorubicin derivatives with intelligent nanogel for improved security and efficacy. *Biomater Sci-UK* 2013;**1**:633-46.

17. Ding J, Xu W, Zhang Y, Sun D, Xiao C, Liu D, et al. Self-reinforced endocytoses of smart polypeptide nanogels for "on-demand" drug delivery. *J Control. Release* 2013;**172**:444-55.

18. Mura S, Nicolas J, Couvreur P. Stimuli-responsive nanocarriers for drug delivery. *Nat Mater* 2013;**12**:991-1003.

19. Ulbrich K, Etrych T, Chytil P, Pechar M, Jelinkova M, Rihova B. Polymeric anticancer drugs with pH-controlled activation. *Int J Pharm* 2004;**277**:63-72.

20. Fang RH, Zhang L. Combinatorial nanotherapeutics: rewiring, then killing, cancer cells. *Sci Signal* 2014;**7**:13.

21. Kelland l. The resurgence of platinum-based cancer chemotherapy. *Nat Rev Cancer* 2007;**7**: 573-84.

22. Cardoso F, Bedard PL, Winer EP, Pagani O, Senkus-Konefka E, Fallowfield LJ, et al. International guidelines for management of metastatic breast cancer: combination *vs* sequential single-agent chemotherapy. *J Natl Cancer I* 2009;**101**:1174-81.

23. Greco F, Vicent MJ. Combination therapy: Opportunities and challenges for polymer-drug conjugates as anticancer nanomedicines. *Adv Drug Deliver Rev* 2009;**61**:1203-13.

24. Ibrahim N, Yu Y, Walsh WR, Yang JL. Molecular targeted therapies for cancer: sorafenib monotherapy and its combination with other therapies (Review). *Oncol Rep* 2012;**27**:1303-11.

25. Wang N, Wang ZG, Xu ZF, Chen XF, Zhu GY. A cisplatin-loaded immunochemotherapeutic nanohybrid bearing immune checkpoint inhibitors for enhanced cervical cancer therapy. *Angew Chem Int Ed* 2018;**57**:3426-30.

26. Li L, Chen C, Liu H, Fu C, Tan L, Wang S, et al. Multifunctional carbon-silica nanocapsules with gold core for synergistic photothermal and chemo-cancer therapy under

the guidance of bimodal imaging. *Adv Funct Mater* 2016;**26**:4252-61.

27. Huang J, Zhang H, Yu Y, Chen Y, Wang D, Zhang G, et al. Biodegradable self-assembled nanoparticles of poly (D,L-lactide-co-glycolide)/hyaluronic acid block copolymers for target delivery of docetaxel to breast cancer. *Biomaterials* 2014;**35**:550-66.

28. Volpi N, Schiller J, Stern R, Soltes L. Role, metabolism, chemical modifications and applications of hyaluronan. *Curr Med Chem* 2009;**16**:1718-45.

29. Toole BP, Wight TN, Tammi MI. Hyaluronan-cell interactions in cancer and vascular disease. *J Biol Chem* 2002;**277**:4593-6.

30. Han X, Li Z, Sun J, Luo C, Li L, Liu Y, et al. Stealth CD44-targeted hyaluronic acid supramolecular nanoassemblies for doxorubicin delivery: Probing the effect of uncovalent pegylation degree on cellular uptake and blood long circulation. *J Control Release* 2015;**197**:29-40.

31. Liemburg-Apers DC, Willems PHGM, Koopman WJH, Grefte S. Interactions between lysosomel reactive oxygen species and cellular glucose metabolism. *Arch Toxicol* 2015;**89**:1209-26.

32. Zhu XY, Yuen MF, Yan L, Zhang ZY, Ai FJ, Yang Y, et al. Diamond-nanoneedle-array-facilitated intracellular delivery and the potential influence on cell physiology. *Adv Healthc Mater* 2016;**5**:1157-68.

33. Li L, Gu W, Chen J, Chen W, Xu ZP. Co-delivery of siRNAs and anti-cancer drugs using layered double hydroxide nanoparticles. *Biomaterials* 2014;**35**:3331-9.

34. Prow TW, Sundh D, Lutty GA. Nanoscale biosensor for detection of reactive oxygen species. *Methods in molecular biology* 2013;**1028**:3-14.

35. Wei WJ, Zhang XJ, Chen XF, Zhou MJ, Xu RR, Zhang XH. Smart surface coating of drug nanoparticles with cross-linkable polyethylene glycol for bio-responsive and highly efficient drug delivery. *Nanoscale* 2016;**8**:8118-25.

36. Varghese OP, Sun W, Hilborn J, Ossipov DA. In situ cross-linkable high molecular weight hyaluronan-bisphosphonate conjugate for localized delivery and cell-specific targeting: a hydrogel linked prodrug approach. *J Am Chem Soc* 2009;**131**:8781.

37. Hermawan A, Wagner E, Roidl A. Consecutive salinomycin treatment reduces doxorubicin resistance of breast tumor cells by diminishing drug efflux pump expression and activity. *Oncol Rep* 2016;**35**:1732-40.

38. Pieniazek A, Czepas J, Piasecka-Zelga J, Gwozdzinski K, Koceva-Chyla A. Oxidative stress induced in rat liver by anticancer drugs doxorubicin, paclitaxel and docetaxel. *Adv Med SCI-POLAND* 2013;**58**:104-111.

39. Wang J, Sun X, Mao W, Sun W, Tang J, Sui M, et al. Tumor redox heterogeneity-responsive prodrug nanocapsules for cancer chemotherapy. *Adv Mater* 2013;**25**:3670-6.

40. Jacquemin G, Margiotta D, Kasahara A, Bassoy EY, Walch M, Thiery J, et al. Granzyme B-induced lysosomel ROS are required for apoptosis. *Cell Death Differ* 2015;**22**:862-74.

41. Zhou H, Fan ZY, Deng JJ, Lemons PLK, Arhontoulis DC, Bowne WB, et al. Hyaluronidase embedded in nanocarrier PEG shell for enhanced tumor penetration and highly efficient antitumor efficacy. *Nano Lett* 2016;**16**:3268-77.

Figure captions

Figure 1. Synthesis route of (A) CAD-PTX and (B) Cys_7-HA-$C18_4$. The regions enclosed by the blue and red frames represent amide bond and ɑ-ethylenic bond, respectively. DOX: doxorubicin; CAD: cis-aconitic anhydride-modified doxorubicin; PTX: paclitaxel; HA: hyaluronic acid.

Figure 2. Schematic illustration of Cys_7-HA-$C18_4$ coated CAD-PTX NPs for drug delivery. CAD-PTX NPs consists of three segments, each defined by the color of its secondary structure: red (CAD), purple (amide bond), and blue (PTX).

Figure 3. Characterization of NPs. (A) SEM and TEM (inset) images of CAD-PTX NPs. The scale bar of the inset image indicates 100 nm; (B) DLS size analysis of CAD-PTX NPs, CAD-PTX-NCLHA NPs and CAD-PTX-CLHA NPs; (C) The evolution of the sizes of different NPs in PBS over a period of 7 days; (D) Amount of free thiol group Cys_7-HA-$C18_4$ (pH 8.5) solution as determined by the Ellman's test; (E, F) Release profiles of DOX from CAD-PTX-CLHA NPs and SAD-PTX-CLHA NPs under different conditions in PBS.

Figure 4. Cellular uptake and intracellular distribution of CAD-PTX-CLHA NPs. Fluorescence images of HeLa cells after being incubated with CAD-PTX-CLHA NPs for different times (4, 6, 12 and 24 h). The scale bars indicate 20 μm. In the figure, red, green, and blue represent NPs, lysosome and nucleus, respectively.

Figure 5. *In vitro* cytotoxicity of CAD-PTX-CLHA NPs. (A, B) Comparative *in vitro* cytotoxicity of CAD-PTX-CLHA NPs against HEK-293T normal cells, A549 and HA pre-treated A549 cancer cells with 24 and 48 h incubation time; (C, D) Cell viabilities of HeLa and 4T1 cells after being incubated with DOX·HCl, PTX, DOX+PTX mixture,

27

CAD-PTX-NCLHA NPs and CAD-PTX-CLHA NPs for 48 h; (E, F) Cell viabilities of MCF-7 and MCF-7/ADR cells after being incubated with DOX·HCl, DOX+PTX mixture and CAD-PTX-CLHA NPs for 48 h.

Figure 6. Inhibition of multidrug resistance with CAD-PTX-CLHA NPs. (A, B) Intracellular distribution of DOX·HCl, and CAD-PTX-CLHA NPs after incubation with MCF-7/ADR cells for 6 and 12 h. Scale bars: 10 μm; (C, D) Flow cytometry analysis of the same groups of experiments as shown in (A, B); (E) Reactive oxygen species (ROS) generation in MCF-7/ADR cells treated with DOX·HCl, PTX, DOX+PTX mixture, and CAD-PTX-CLHA NPs for 12 and 24 h. Scale bars: 20 μm.

Figure 7. *In vivo* performance of CAD-PTX-CLHA NPs. (A) *In vivo* fluorescence image of a tumor bearing mouse at 24 h post injection of CAD-PTX-CLHA NPs; (B) Biodistribution of CAD-PTX-CLHA NPs; the inset figure is the fluorescence image of major organs at 24 h after NP injection; The evolution of tumor volumes (C) and body weight (D) with time after mice were administered with saline, DOX·HCl, PTX, DOX+PTX mixture and CAD-PTX-CLHA NPs.

Figure 1.
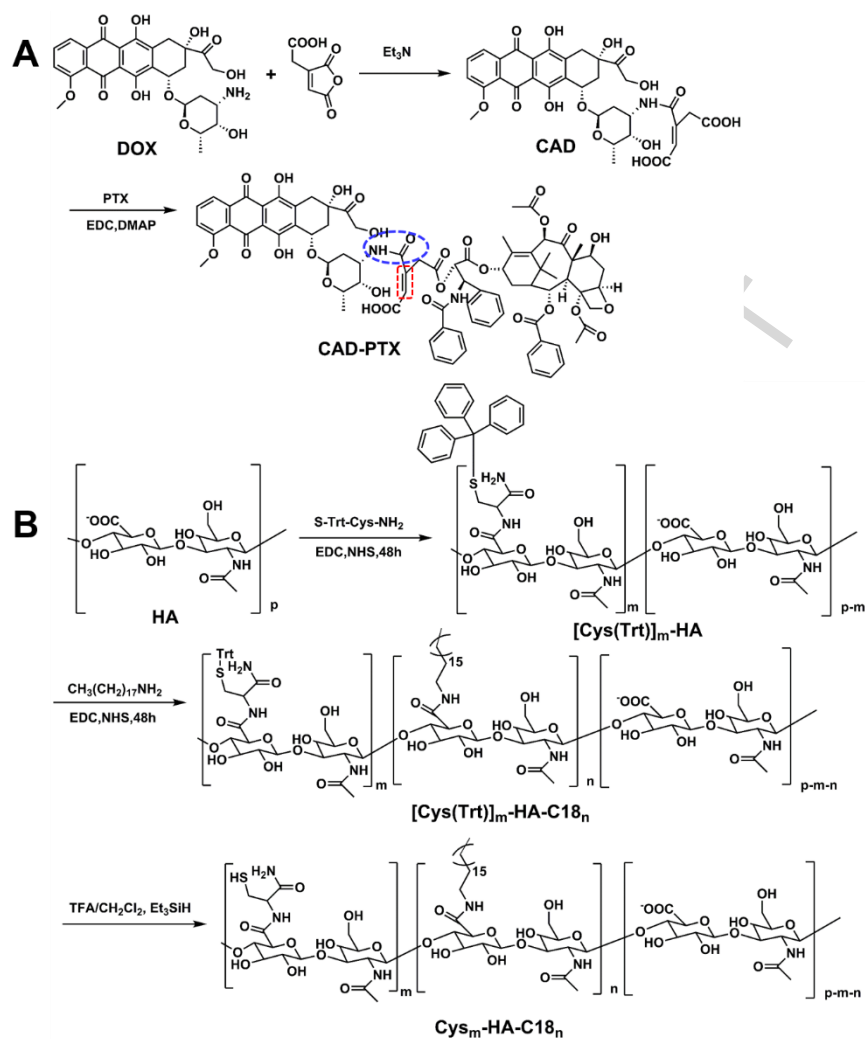
Figure 2.
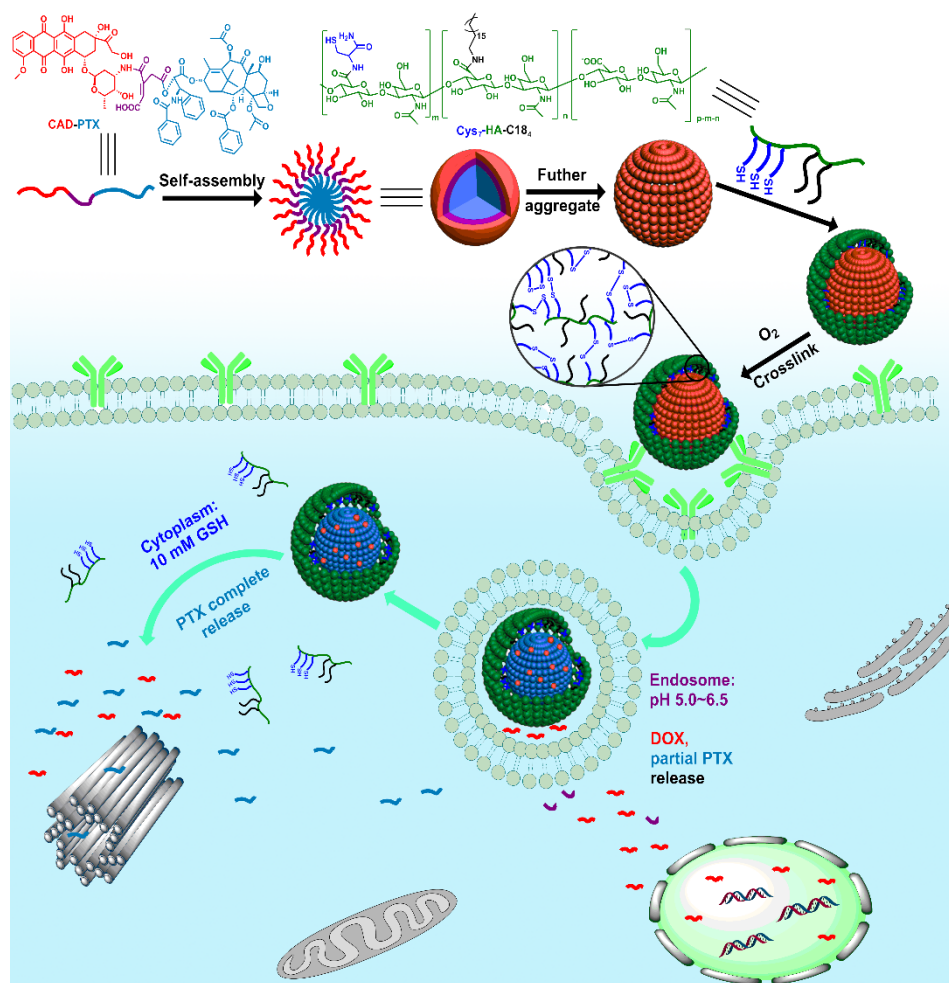
Figure 3.
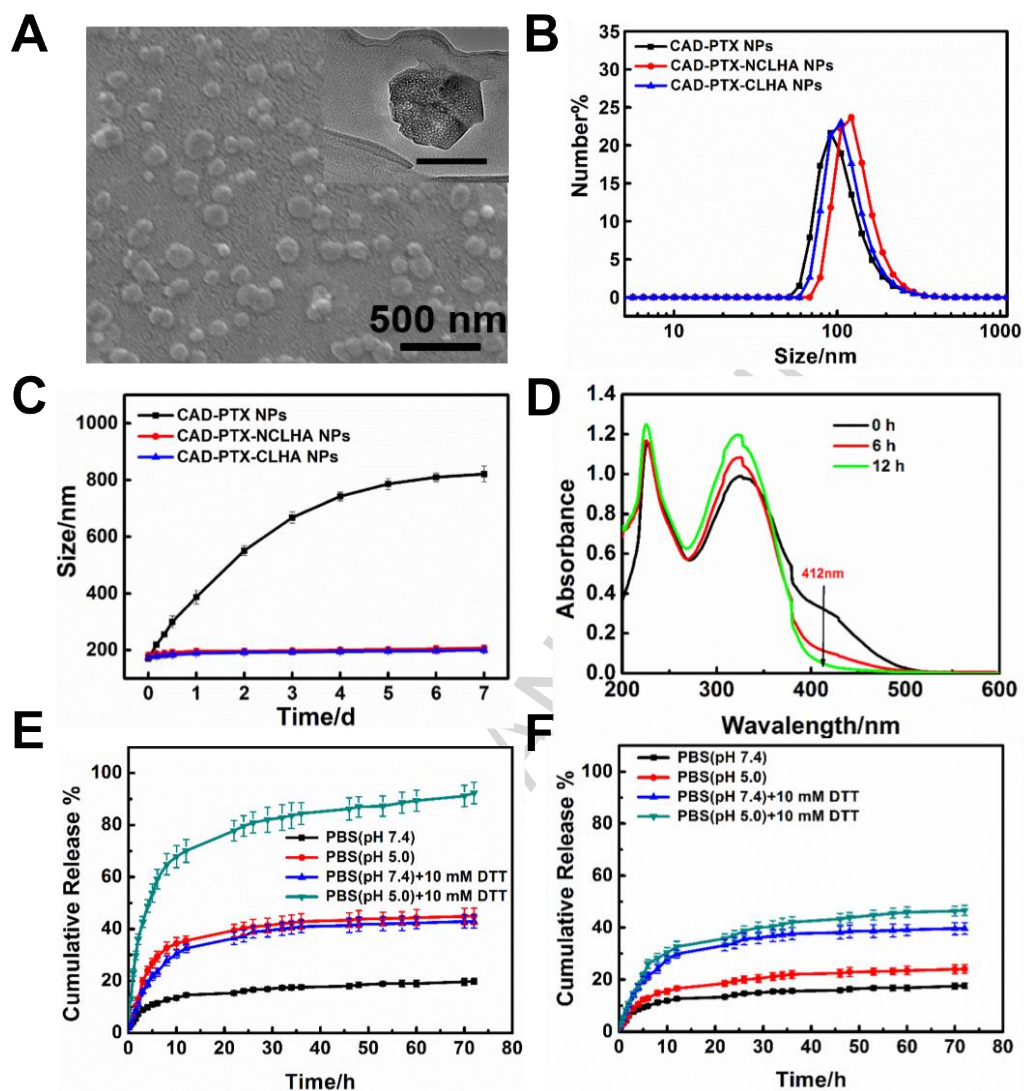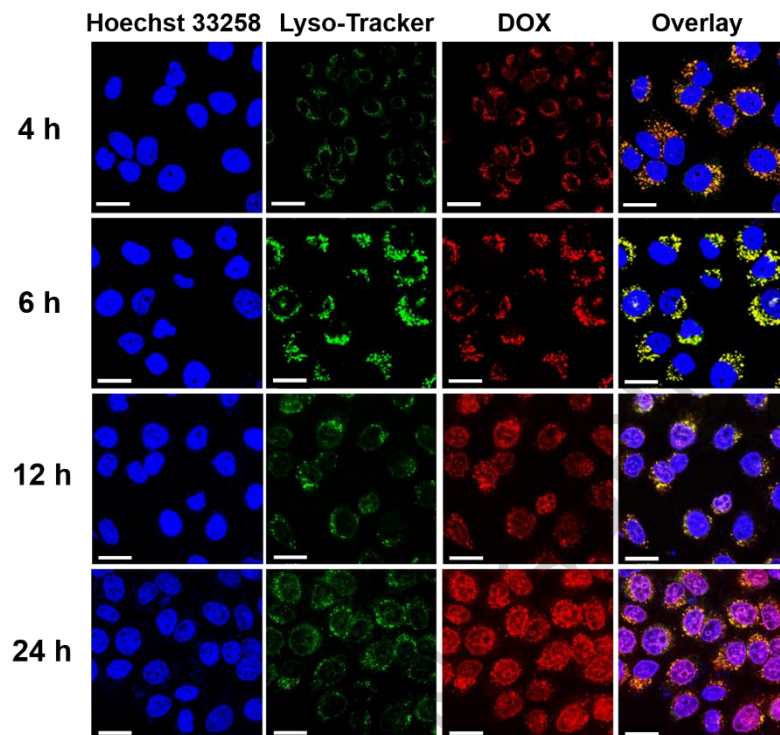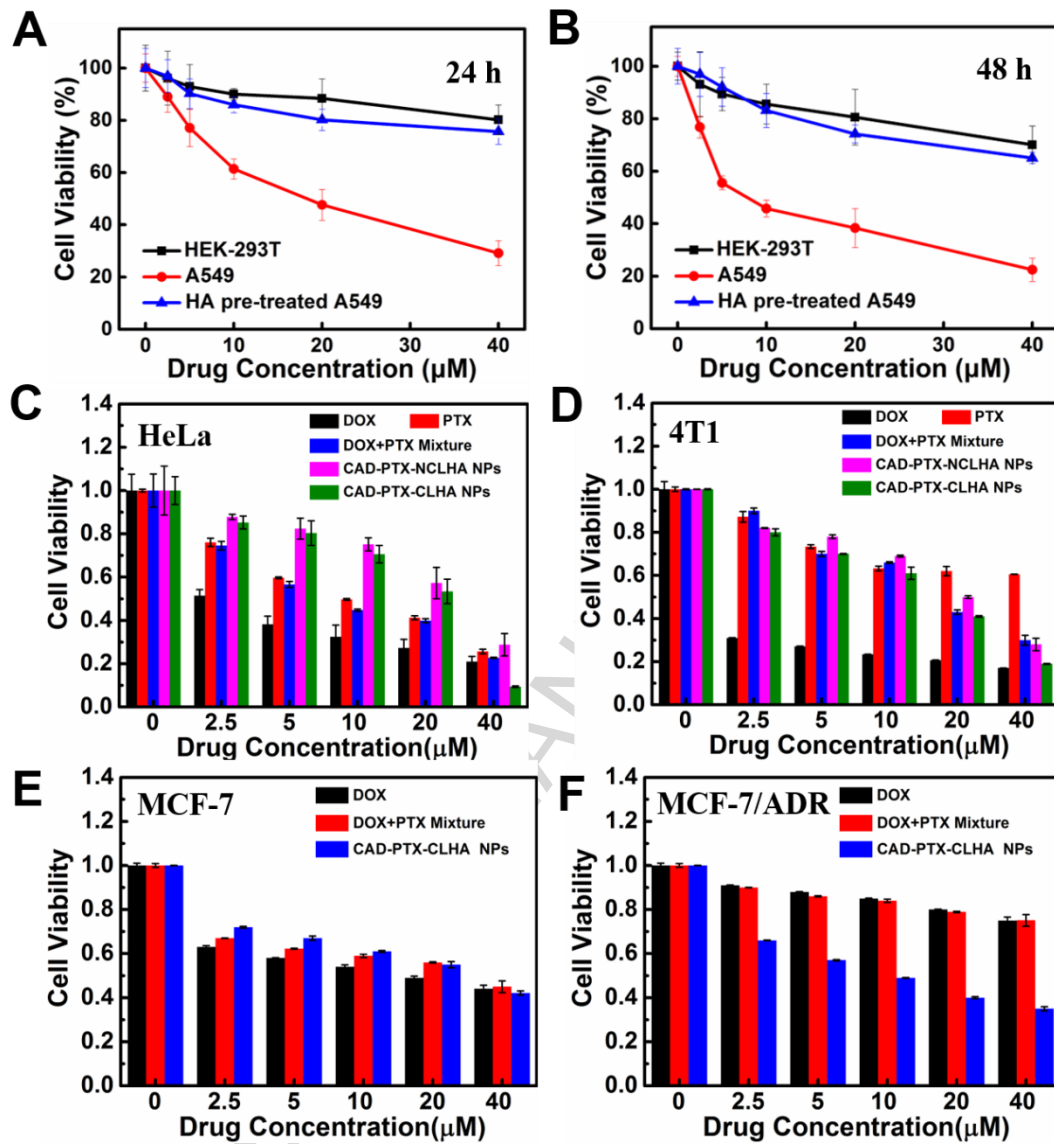
Figure 4.
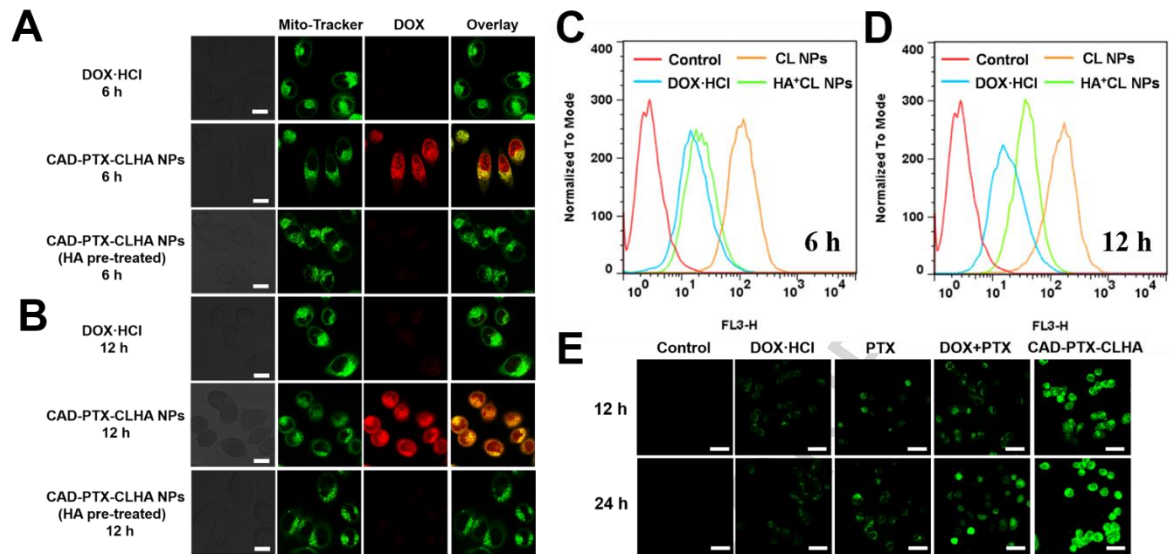
Figure 5.

Figure 6.

Figure 7.
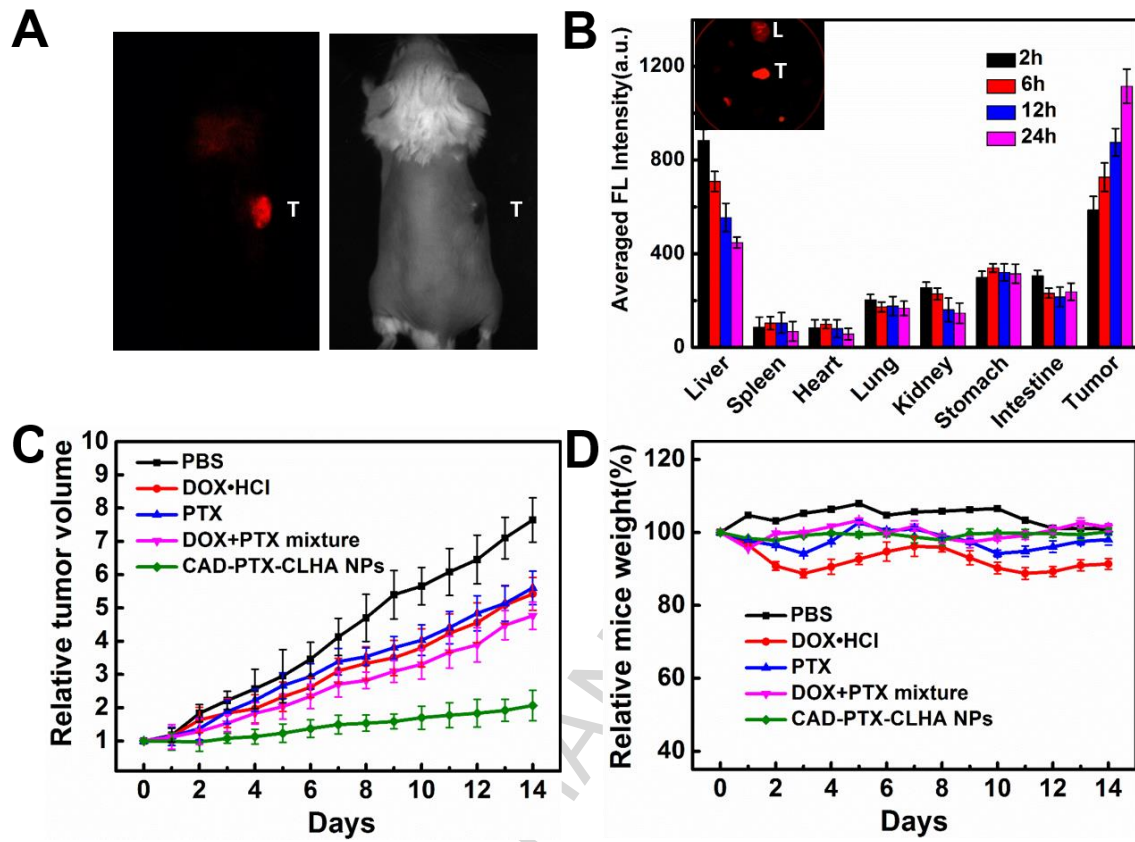
We covalently conjugate cis-aconitic anhydride-modified doxorubicin and paclitaxel (CAD-PTX) and then self-assemble to nanoparticles, followed by coating with crosslinked hyaluronic acid (HA) via disulfide bonds. These NPs possesses pH-and redox- dual responsive release characteristics. Besides, the drug system is able to target cancer cells with overexpression of CD44 receptor and possesses potent toxicity to multidrug resistant cells.

Graphical Abstract

Figure 1

Figure 2

Figure 3

Figure 4

Figure 5

Figure 6

Figure 7